arXiv:1611.06315v1 [astro-ph.CO] 19 Nov 2016

Observational constraints on the generalized α attractor model

M. Shahalam[1], Ratbay Myrzakulov[2], Shynaray Myrzakul[3], Anzhong Wang[4]
[1,4]*Institute for Advanced Physics & Mathematics, Zhejiang University of Technology, Hangzhou, 310032, China*
[2]*Eurasian International Center for Theoretical Physics, Department of General and Theoretical Physics, Eurasian National University, Astana, Kazakhstan*
[3]*Department of Theoretical and Nuclear Physics, Al-Farabi Kazakh National University, Al-Farabi Almaty, Kazakhstan*

We study the generalized α attractor model in context of late time cosmic acceleration; the model interpolates between freezing and thawing dark energy models. In the slow roll regime, the originally potential is modified whereas the modification ceases in the asymptotic regime and the effective potential behaves as quadratic. In our setting, field rolls slowly around the present epoch and mimics dark matter in future. We put observational constraints on the model parameters for which we use an integrated data base (SN+Hubble+BAO+CMB) for carrying out the data analysis.

I. INTRODUCTION

The past two decades of tremendous activities in observational cosmology motivated the theorists to rethink about the formulation of theory of gravity. This leads to a plethora of cosmological models at theoretical ground. The observations of Type Ia supernovae by the Supernova Cosmology Project and the High-Z Supernova Search Team gave significant results about the accelerated expansion of the Universe (against the presumed decelerating expansion caused by gravity) for which the three members of these groups awarded Nobel Prize for their discovery. Baryon acoustic oscillations and some other new results about the clustering of galaxies gave more confirmatory evidence to this fact. Nowadays the concept of late time cosmic acceleration has become a fundamental ingredient for the theorists in modelling the Universe. The idea of late time cosmic acceleration is mainly attributed to the presence of some mysterious entity commonly referred to as Dark energy [1–3]. Although there have been developed several ideas to explain the cosmic acceleration, the theory of Dark Energy is much more successful to explaining various phenomena. On the other hand primordial inflation has taken a special status in explaining the origin of the anisotropies in the cosmic microwave background radiation (CMBR) and the formation of large scale structures. The origin of both early and late time inflation still represents a great theoretical puzzle which motivated theorists to invoke scalar field to explain the two inflationary phases simultaneously. During the past three and half decades, a wide variety of inflationary theories have been proposed among which "cosmological attractors" was discovered very recently. These are very broad class which incorporates the conformal attractors [4], alpha attractors [5] and also includes the scalar field cosmological models such as Starobinsky model [6], the chaotic inflation in super-gravity (GL model) [7], Higgs inflation [8] and axion monodromy inflationary models [9]. All these have a mysterious fact in the context of recently released results obtained by WMAP and Planck data [10] that they provide the very similar cosmological predictions although they have different origins. For conformal attractors, they predict that, for large number of e-foldings N, the spectral index and tensor-to-scalar ratio are given by $n_s = 1 - 2/N$; $r = 12/N^2$. For $N \sim 60$, these predictions are $n_s \sim 0.967, r \sim 0.003$ while for $N \sim 50$, $n_s \sim 0.96, r \sim 0.005$ which are in very good agreement with WMAP and Planck data. For α attractors, the slow roll parameters n_s and r can be written as $-$ for small α, $n_s = 1 - 2/N, r = 12\alpha/N^2$ and for large α, $n_s =$ practically does not change, $r = 12\alpha/(N(N + 3\alpha/2))$, where N is the number of e-foldings between the end of inflation and the inflationary horizon, and the numerical values lies in the range $50 \leq N \leq 60$. These models have some more features besides the inflation that they can be used to explain the late time cosmic acceleration and also the super-symmetry breaking [11].

The paper is organized as follows. In Section II, we present the basics of α attractor models and establish them to a class of models. Section III displays the evolution equations of scalar field in the autonomous form and addresses the cosmological attractor behaviour. In Section IV, we use joint data to carry out the observational analysis and put constraints on the model parameters. Our results are concluded in Section V.

II. α - MODELS

Here, we focus on the minimally coupled alpha attractors which are of more interest as they play an interesting role in cosmology to investigate the dark energy properties and try to evaluate if these models can explain the late time cosmic acceleration. In the Einstein frame, the Lagrangian density of the alpha attractor model takes the following form,

$$\mathcal{L} = \sqrt{-g}\left[\frac{1}{2}M_p^2 R - \frac{\alpha}{\left(1-\frac{\varphi^2}{6}\right)^2}\frac{(\partial\varphi)^2}{2} - \alpha f^2\left(\frac{\varphi}{\sqrt{6}}\right)\right] \tag{1}$$

with a real scalar field φ. Despite of the changes in the inflaton potential and arbitrary function $f(\varphi)$ these class of models have same striking results for primordial scalar perturbation tilt and the tensor to scalar power ratio. For $\alpha = 1$, the Starobinsky model is recovered. We should note that the kinetic and potential energies both have overall coefficient α. One can observe that the kinetic term is not canonical which can be so through a field redefinition $\phi = \sqrt{6\alpha}\tanh^{-1}\left(\frac{\varphi}{\sqrt{6}}\right)$ and the potential function $V(\phi) = \alpha f^2\left(\tanh\left(\frac{\phi}{\sqrt{6\alpha}}\right)\right)$ with vanishing field at $\phi = \infty$. We are interested in the dynamics of the scalar field and its evolution of equation of state and see whether it explains the late-time cosmic acceleration.

Two functional forms of f have been employed for inflation namely,

$$f = c\,\tanh\left(\frac{\phi}{\sqrt{6\alpha}}\right), \tag{2}$$

$$\text{and} \qquad f = c\,\frac{\tanh\left(\frac{\phi}{\sqrt{6\alpha}}\right)}{1+\tanh\left(\frac{\phi}{\sqrt{6\alpha}}\right)} \tag{3}$$

The first one is known as the T model and the second one is the Starobinsky model (α=1). Both the models are identical at small ϕ and give quadratic potential near the origin.

We consider a generalized α model given by [12]

$$f = c\,\frac{\tanh\left(\frac{\phi}{\sqrt{6\alpha}}\right)}{\tanh\left(\frac{\phi}{\sqrt{6\alpha}}\right)^n} \tag{4}$$

where c is a constant and scales the amplitude of the potential, α is a parameter which scales the field ϕ, and n is an integer which takes the values 0,1,2,3 etc. Therefore, the potential of the generalized α model becomes

$$V(\phi) = \alpha\, c^2\,\frac{\tanh\left(\frac{\phi}{\sqrt{6\alpha}}\right)^2}{\tanh\left(\frac{\phi}{\sqrt{6\alpha}}\right)^n} \tag{5}$$

As $\phi \to \infty$ (maximum value), the potential becomes constant (flatten), and as $\phi \to 0$ (minimum value), it behaves as a quadratic potential (see figure 1).

III. EVOLUTION EQUATIONS AND ATTRACTORS

Caldwell and textcolorredLinder [13] revealed that the scalar field models can be divided into two big categories: the fast roll (freezing) and slow roll (thawing) models. A freezing model is such that, during the matter/radiation era, the field mimics the background and remains sub-dominant. Only at late times, the field exits to late time cosmic acceleration. The freezing models remain independent for a wide range of initial conditions. In contrast, the thawing models are alike to inflaton that derives acceleration at early epoch. in the thawing class of models, the scalar field is initially frozen due to large Hubble damping and behaves as a cosmological constant with $w \approx -1$. At late times the Hubble damping decreases and the scalar field slowly thaws from the frozen state and deviates from the cosmological constant kind behavior. Thawing models are much sensitive to initial conditions. Some of the models of these classes have been studied in references [14, 15].

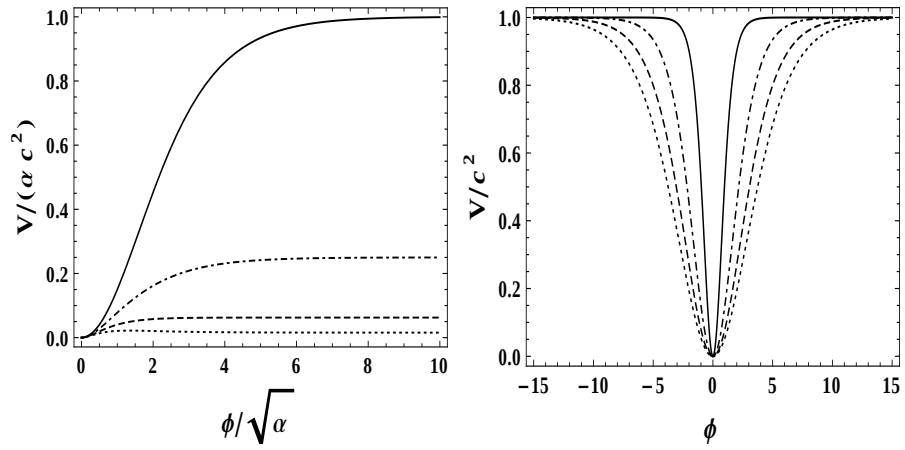

FIG. 1: In the left panel, the potential (5) of the generalize α model is plotted against $\phi/\sqrt{\alpha}$, for $n = 0, 1, 2, 3$. For large field values ($\phi \gg \sqrt{\alpha}$), the potential becomes constant and for small field values ($\phi \ll \sqrt{\alpha}$), it behaves as a quadratic potential. The right panel shows the evolution of potential versus field ϕ, for different values of α. The dot, dashed, dot-dashed and solid lines represent the values of $\alpha = 3, 2, 1$ and 0.2 respectively. The smaller α corresponds to more narrow minima of the potentials. This panel is plotted only for $n = 0$. In both panels, the potential and field are shown in units of c^2 and planck, respectively.

The α attractor models seem to combine these two classes in one way. We consider the potential given by equation (5), which has the following asymptotic form

$$V(\phi) \approx \alpha\ c^2\ 2^{-2n} \left(1 - 2(2-n)e^{-\frac{2\phi}{\sqrt{6\alpha}}}\right), \qquad \phi \gg \sqrt{\alpha} \tag{6}$$

This is an uplifted exponential potential and studied as the inflation models [7]. The exponential potential falls in the freezing class and approaches to a cosmological constant.

$$V(\phi) \approx \frac{c^2}{6\alpha}\phi^2, \qquad \phi \ll \sqrt{\alpha} \tag{7}$$

This is the quadratic potential, falls in the thawing class and deviates from the cosmological textcolorredconstant. In this case, as ϕ approaches the origin, the time average equation of state during the oscillations is given as $< w >= 0$ (in future).

The equations of motion are obtained by varying the Lagrangian density (1) with equation (5) have the following form

$$\frac{\dot{a}^2(t)}{a^2(t)} \ = \ \frac{1}{3M_{pl}^2}\left(\rho_r + \rho_m + \rho_\phi\right) \tag{8}$$

$$\ddot{\phi} + 3\frac{\dot{a}}{a}\dot{\phi} + V'(\phi) = 0 \tag{9}$$

where prime ($'$) denotes derivative with respect to ϕ. In the discussion to follow we shall use the dimensionless variables

$$Y_1 = \frac{\phi}{M_p}, \quad Y_2 = \frac{\dot{\phi}}{M_p H_0}, \quad \mathcal{V} = \frac{V(Y_1)}{M_p^2 H_0^2}. \tag{10}$$

Using the new dimensionless variables, we can cast equations (8) and (9) as a system of first order equations

$$Y_1' = \frac{Y_2}{h(Y_1, Y_2)} \tag{11}$$

$$Y_2' = -3Y_2 - \frac{1}{h(Y_1, Y_2)}\Big[\frac{d\mathcal{V}(Y_1)}{dY_1}\Big] \tag{12}$$

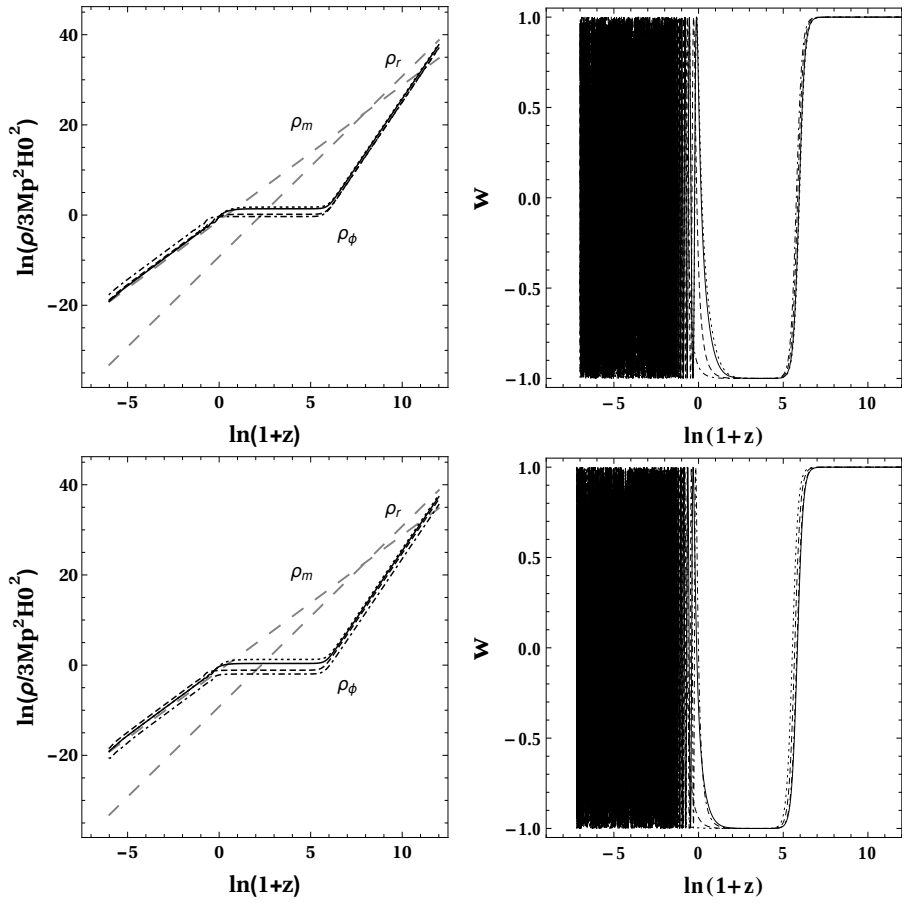

FIG. 2: The figure exhibits the evolution of energy density ρ and equation of state w versus redshift z. The dot-dashed, dashed, solid, and dotted lines correspond to the energy density of scalar field ρ_ϕ and w for various values of $\alpha = 0.05, 0.1, 1$ and 10, respectively. The upper and lower left panels show that, initially, the field energy density ρ_ϕ is highly sub-dominant and remains so for almost all of the period of evolution. At late times, ρ_ϕ catches up with the energy density of background (large gray dashed lines) and overtakes it. Around the present epoch, ρ_ϕ scales with the background and in far future it exits from the background. The upper and lower right panels show the evolution of equation of state w for a scalar field. In the future, the equation of state oscillates between $+1$ and -1, and the system pass most of the time around $w = \pm 1$. Here we use $\Omega_{0m} = 0.3$ and $c = 7M_pH_0$. The upper panels are for $n = 0$ whereas lower panels are for $n = 1$.

The prime ($'$) denotes the derivative with respect to $\ln(a)$, and the function $h(Y_1, Y_2)$ is given by:

$$h(Y_1, Y_2) = \sqrt{\left[\frac{Y_2^2}{6} + \frac{\mathcal{V}(Y_1)}{3} + \Omega_{0m}e^{-3a} + \Omega_{0r}e^{-4a}\right]} \tag{13}$$

Here, Ω_{0r} and Ω_{0m} are the energy density parameters of radiation and matter, respectively at the present epoch. The results are shown in figures 1 - 3 after solving the evolution equations (11) and (12), numerically. Figure 1 exhibits the behavior of potential (5) versus field ϕ, in units of c^2 and planck, respectively. The left panel is plotted for $n = 0, 1, 2, 3$. For large field values, the potential flattens to an uplifted plateau, while at small values it looks like the quadratic potential. The right panel is plotted for $n = 0$ with various values of α. The smaller values of α correspond to more narrow minima of the potentials.

As the field evolving from the flatten region approaches the origin, the energy density ρ_ϕ undershoots the background and begins as thawing dark energy along with thawing behaviour as the field freezes due to large Hubble damping, and even it lies in the thawing region at present epoch. However in the future it switches over and converts to freezing behaviour, towards the cosmological attractor (see figure 2).

The upper and lower right panels of figure 2 show that the field oscillates most of the time between $w = \pm 1$ and correspondingly the average equation of state $< w >= 0$ at the attractor point (see figure 3) which is consistent with the analytical result for quadratic potential.

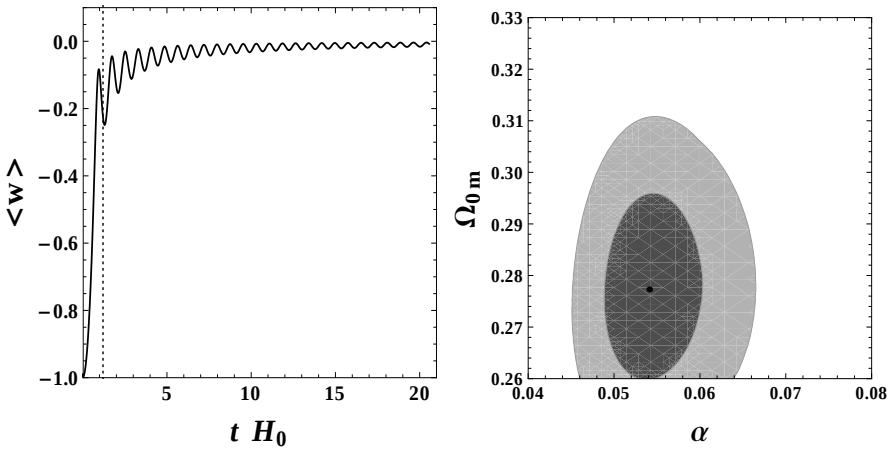

FIG. 3: The left panel displays the average equation of state versus the cosmic time, in the far future, the potential behaves as a quadratic potential whose average equation of state $< w >= 0$ at attractor point that is shown in this panel. The vertical dotted line represents the present epoch. The right panel shows 1σ (dark shaded) and 2σ (light shaded) likelihood contours for the generalized α model. We have used joint data (SN + Hubble + BAO + CMB) to carry out the data analysis. The black dot represents the best-fitting values of the parameters, which are found to be $\alpha = 0.054$ and $\Omega_{0m} = 0.28$.

The right panel of figure 3 demonstrates the 1σ (dark shaded) and 2σ (light shaded) likelihood contours in the $\alpha - \Omega_{0m}$ plane, for the generalized α attractor model. The joint data (SN+Hubble+BAO+CMB) has been used for carrying out the observational analysis. The best-fitting values of the model parameters are found to be $\alpha = 0.054$ and $\Omega_{0m} = 0.28$.

IV. DATA ANALYSIS

We employ the χ^2 analysis to constrain the model parameters. One can use the maximum likelihood method and get the total likelihood for the parameters α and Ω_{0m} as the product of individual likelihood for different datasets. The total likelihood function for joint data is given by

$$\mathcal{L}_{tot}(\alpha, \Omega_{0m}) = e^{-\frac{\chi^2_{tot}(\alpha,\Omega_{0m})}{2}} \tag{14}$$

where

$$\chi^2_{\rm tot} = \chi^2_{\rm SN} + \chi^2_{\rm Hub} + \chi^2_{\rm BAO} + \chi^2_{\rm CMB}\,, \tag{15}$$

is related to Type Ia supernova (SN), data of Hubble parameter, Baryon Acoustic Oscillation (BAO) and Cosmic Microwave Background (CMB) data. The best fit value of the parameters is acquired by minimizing $\chi^2_{\rm tot}$ with respect to α and Ω_{0m}. The likelihood contours in 1σ and 2σ confidence level are given as 2.3 and 6.17, respectively, in the two dimensional parametric space.

A. Type Ia Supernova

To study the Universe on a very large scale, Type Ia supernova is considered as an ideal astronomical object. They are very bright and the luminosity distance can be determined upto the redshift $z \simeq 1.4$. They have almost the same luminosity which is redshift-independent. Hence Type Ia supernova are observed as very good standard candles.

The Type Ia supernova is one of the direct probe for the cosmological expansion. We take 580 data points of latest Union2.1 compilation data [16]. In this case, one measures the apparent luminosity of the supernova explosion. The most appropriate quantity is the luminosity distance $D_L(z)$ defined as

$$D_L(z) = (1+z)\int_0^z \frac{H_0 dz'}{H(z')}. \tag{16}$$

In reality, the distance modulus $\mu(z)$ is the observed quantity which is directly related to the $D_L(z)$ as $\mu(z) = m - M = 5\log D_L(z) + \mu_0$, where M and m are the absolute and apparent magnitudes of the

Supernovae and $\mu_0 = 5\log\left(\frac{H_0^{-1}}{\rm Mpc}\right) + 25$ is a nuisance parameter which should be marginalized. Therefore, the corresponding χ^2 can be written as

$$\chi^2_{\rm SN}(\mu_0, \theta) = \sum_{i=1}^{580} \frac{\left[\mu_{th}(z_i, \mu_0, \theta) - \mu_{obs}(z_i)\right]^2}{\sigma_\mu(z_i)^2}\,, \tag{17}$$

where μ_{obs}, μ_{th} and σ_μ represent the observed, theoretical distance modulus and uncertainty in the distance modulus respectively; θ represents any arbitrary parameter of the particular model. Eventually marginalizing μ_0 and following reference [17], we get

$$\chi^2_{\rm SN}(\theta) = A(\theta) - \frac{B(\theta)^2}{C(\theta)}\,, \tag{18}$$

where,

$$A(\theta) = \sum_{i=1}^{580} \frac{\left[\mu_{th}(z_i, \mu_0 = 0, \theta) - \mu_{obs}(z_i)\right]^2}{\sigma_\mu(z_i)^2}\,, \tag{19}$$

$$B(\theta) = \sum_{i=1}^{580} \frac{\mu_{th}(z_i, \mu_0 = 0, \theta) - \mu_{obs}(z_i)}{\sigma_\mu(z_i)^2}\,, \tag{20}$$

$$C(\theta) = \sum_{i=1}^{580} \frac{1}{\sigma_\mu(z_i)^2}\,. \tag{21}$$

B. The Hubble Parameter $H(z)$

The Hubble Parameter $H(z)$ represents the expansion history of the Universe and plays a key role in joining the cosmological models and observations. Recently, Farooq and Ratra [18] compiled 28 data points for $H(z)$ in the redshift range $0.07 \leq z \leq 2.3$ which are given in Table I. To complete the data set we take $H_0 = 67.3 \pm 1.2\ Km/S/M_{Pc}$ from Planck 2013 results [19]. We shall work with the normalized Hubble parameter, $h = H/H_0$ and apply the data to the model. In this case, the χ^2 is defined as

$$\chi^2_{\rm Hub}(\theta) = \sum_{i=1}^{29} \frac{\left[h_{\rm th}(z_i, \theta) - h_{\rm obs}(z_i)\right]^2}{\sigma_h(z_i)^2}\,, \tag{22}$$

where $h_{\rm obs}$ and $h_{\rm th}$ are respectively the observed and theoretical values of the normalized Hubble parameter. Also,

$$\sigma_h = \left(\frac{\sigma_H}{H} + \frac{\sigma_{H_0}}{H_0}\right) h, \tag{23}$$

where σ_H and σ_{H_0} are the errors associated with H and H_0 respectively.

C. Baryon Acoustic Oscillation (BAO)

The early Universe composed of photons, baryons and dark matter. Photons and baryons are tightly coupled to one another through Thompson scattering, and act as a single fluid. This fluid can not collapse under gravity but it can oscillate, due to the large pressure furnished by the photons. These oscillations are known as BAO, which are the consequences of photon-baryon coupling at redshift larger than $z = 1090$.

The characteristic scale of these oscillations is governed by the sound horizon r_s at the photon decoupling epoch, given as:

$$r_s(z_*) \;=\; \frac{c}{\sqrt{3}} \int_0^{\frac{1}{1+z_*}} \frac{da}{a^2 H(a)\sqrt{1 + (3\Omega_{0b}/4\Omega_{0\gamma})a}}, \tag{24}$$

where Ω_{0b} and $\Omega_{0\gamma}$ are the present values of baryon and photon density parameter respectively, and z_* is the redshift of photon decoupling.

TABLE I: $H(z)$ measurements (in unit [km s^{-1}Mpc^{-1}]) and their errors [18].

z	$H(z)$ (km/s/Mpc)	σ_H (km/s/Mpc)	Reference
0.070	69	19.6	[20]
0.100	69	12	[21]
0.120	68.6	26.2	[20]
0.170	83	8	[21]
0.179	75	4	[22]
0.199	75	5	[22]
0.200	72.9	29.6	[20]
0.270	77	14	[21]
0.280	88.8	36.6	[20]
0.350	76.3	5.6	[23]
0.352	83	14	[22]
0.400	95	17	[21]
0.440	82.6	7.8	[24]
0.480	97	62	[25]
0.593	104	13	[22]
0.600	87.9	6.1	[24]
0.680	92	8	[22]
0.730	97.3	7.0	[24]
0.781	105	12	[22]
0.875	125	17	[22]
0.880	90	40	[25]
0.900	117	23	[21]
1.037	154	20	[22]
1.300	168	17	[21]
1.430	177	18	[21]
1.530	140	14	[21]
1.750	202	40	[21]
2.300	224	8	[26]

The BAO sound horizon scale can be used to derive the angular diameter distance D_A and the Hubble expansion rate H as a function of redshift. By measuring the subtended angle $\Delta\theta$, of the ruler of length r_s, these parameters are defined as follows:

$$\Delta\theta \;=\; \frac{r_s}{d_A(z)} \qquad \text{with} \qquad d_A(z) = \int_0^z \frac{dz'}{H(z')} \tag{25}$$

where $\Delta\theta$ is the measured angular separation of the BAO feature in the 2 point correlation function of the galaxy distribution on the sky, and

$$\Delta z \;=\; H(z) r_s, \tag{26}$$

where Δz is the measured redshift separation of the BAO feature in the 2 point correlation function along the line of sight. We work with BAO data of $d_A(z_\star)/D_V(Z_{BAO})$ [27–32], where $z_\star \approx 1091$ is the decoupling time, $d_A(z)$ is the co-moving angular-diameter distance and $D_V(z) = \left(d_A(z)^2 z/H(z)\right)^{1/3}$ is the dilation scale. Data needed for this inspection is shown in Table II. The corresponding $\chi^2_{\rm BAO}$ is given as [32]:

$$\chi^2_{\rm BAO} = X^T C^{-1} X\,, \tag{27}$$

where

$$X = \begin{pmatrix} \frac{d_A(z_\star)}{D_V(0.106)} - 30.95 \\ \frac{d_A(z_\star)}{D_V(0.2)} - 17.55 \\ \frac{d_A(z_\star)}{D_V(0.35)} - 10.11 \\ \frac{d_A(z_\star)}{D_V(0.44)} - 8.44 \\ \frac{d_A(z_\star)}{D_V(0.6)} - 6.69 \\ \frac{d_A(z_\star)}{D_V(0.73)} - 5.45 \end{pmatrix}, \tag{28}$$

TABLE II: Values of $\frac{d_A(z_\star)}{D_V(Z_{BAO})}$ for distinct values of z_{BAO}.

z_{BAO}	0.106	0.2	0.35	0.44	0.6	0.73
$\frac{d_A(z_\star)}{D_V(Z_{BAO})}$	30.95 ± 1.46	17.55 ± 0.60	10.11 ± 0.37	8.44 ± 0.67	6.69 ± 0.33	5.45 ± 0.31

and C^{-1} is the inverse covariance matrix defined as in [32].

$$C^{-1} = \begin{pmatrix} 0.48435 & -0.101383 & -0.164945 & -0.0305703 & -0.097874 & -0.106738 \\ -0.101383 & 3.2882 & -2.45497 & -0.0787898 & -0.252254 & -0.2751 \\ -0.164945 & -2.45499 & 9.55916 & -0.128187 & -0.410404 & -0.447574 \\ -0.0305703 & -0.0787898 & -0.128187 & 2.78728 & -2.75632 & 1.16437 \\ -0.097874 & -0.252254 & -0.410404 & -2.75632 & 14.9245 & -7.32441 \\ -0.106738 & -0.2751 & -0.447574 & 1.16437 & -7.32441 & 14.5022 \end{pmatrix}. \tag{29}$$

D. Cosmic Microwave Background (CMB) distance information

The CMB measurement is sensitive to distance to the last scattering surface (decoupling epoch) via the positions of peaks and troughs of acoustic oscillations. Following the WMAP results [33], the distance information incorporates the "shift parameter" R, "acoustic scale" l_A and the redshift of last scattering surface z_{ls}, where R and l_A are the ratio of angular diameter distance to the last scattering surface epoch over the Hubble horizon and the sound horizon at surface of the last scattering, and are given by

$$R = H_0\sqrt{\Omega_{0m}}\,\chi(z_{ls}), \tag{30}$$

$$l_A = \frac{\pi\chi(z_{ls})}{\chi_s(z_{ls})}, \tag{31}$$

where $\chi(z_{ls})$ is the co-moving distance to z_{ls} and $\chi_s(z_{ls})$ is the co-moving sound horizon at z_{ls}. The shift parameter R can also be computed theoretically using the formula

$$R = H_0\sqrt{\Omega_{0m}}\int_0^{z_{ls}}\frac{dz'}{H(z')}. \tag{32}$$

From equation (32), we observe that R is related to the matter density as well as the expansion history of the Universe until the redshift of the surface of the last scattering, z_{ls}, which is computed through the fitting function [34]:

$$z_{ls} = 1048\left[1 + 0.00124(\Omega_b h^2)^{-0.738}\right]\left[1 + g_1(\Omega_{0m}h^2)^{g_2}\right], \tag{33}$$

where g_1 and g_2 are defined as

$$g_1 = \frac{0.0783(\Omega_b h^2)^{-0.238}}{1 + 39.5(\Omega_b h^2)^{0.763}}, \tag{34}$$

$$g_2 = \frac{0.56}{1 + 21.1(\Omega_b h^2)^{1.81}}. \tag{35}$$

The corresponding χ^2 can be written as

$$\chi^2(\theta) = \frac{(R(\theta) - R_0)^2}{\sigma^2}, \tag{36}$$

where $R(\theta)$ depends on the model parameter θ and $R_0 = 1.725 \pm 0.018$ [33].

V. CONCLUSION

In this paper, we have investigated the generalized α attractor model that leads to cosmological attractor behavior and can interpolate between thawing and freezing models. At the present epoch, it behaves as a thawing model whereas in the future it shows freezing behavior. In figure 2, the dynamics of the energy density ρ_ϕ is shown for $\alpha = 0.05, 0.1, 1$ and 10, with common general characteristics. The evolution of ρ_ϕ starts off as thawing dark energy along with thawing behavior and even at the present epoch it lies in the thawing region. But in the future it switches over and turns to scaling regime which is cosmological attractor. For small values of the field ϕ, the generalized α attractor model mimics the power law behavior $V(\phi) \sim \phi^2$ and produces oscillations of ϕ near the origin which are reflected in the behavior of the equation of state w (see figure 2) and correspondingly the average equation of state parameter $< w >= 0$ (see figure 3). In our setting, field remains in the slow roll region but mimics dark matter in future. We have used joint data (SN+Hubble+BAO+CMB) for observational analysis. The best fit values of the model parameters are found to be $\alpha = 0.054$ and $\Omega_{0m} = 0.28$.

Acknowledgements

M.S. thanks M. Sami for making useful comments and suggestions. He is also thankful to M. Sajjad Athar for his constant encouragement throughout the work. A.W. is supported in part by NNSFC No.11375153 and No. 11675145, China.

[1] E. J. Copeland, M. Sami, S. Tsujikawa, Int. J. Mod. Phys. D 15, 1753 (2006) [arXiv:hep-th/0603057].
[2] V. Sahni, A. A. Starobinsky, Int. J. Mod. Phys. D 9, 373 (2000) [astro-ph/9904398].
[3] M. Sami, New Adv. Phys. 10 (2016) 77-105 [arXiv:1309.4188]; M. Sami, R. Myrzakulov, Int.J.Mod.Phys. D25 (2016) no.12, 1630031 [arXiv:1309.4188]; M. Sami, Curr. Sci. 97 (2009) 887 [arXiv:hep-th/0904.3445]; M Sami, arXiv:0901.0756v1 (2009); Md. Wali Hossain et al., Int. J. Mod. Phys. D 24 1530014 (2015) [arXiv:1410.6100]; M. Sami, N. Dadhich, TSPU Vestnik 44N7 (2004) 25-36 [arXiv:hep-th/0405016].
[4] R. Kallosh and A. Linde, JCAP 1307, 002 (2013) [arXiv:1306.5220 [hep-th]]. R. Kallosh and A. Linde, JCAP 1312, 006 (2013) [arXiv:1309.2015 [hep-th]].
[5] D. I. Kaiser and E. I. Sfakianakis, Phys. Rev. Lett. 112, no. 1, 011302 (2014) [arXiv:1304.0363 [astro-ph.CO]]. S. Ferrara, R. Kallosh, A. Linde and M. Porrati, Phys. Rev. D 88, no. 8, 085038 (2013) [arXiv:1307.7696 [hep-th]]. R. Kallosh, A. Linde and D. Roest, JHEP 1311, 198 (2013) [arXiv:1311.0472 [hep-th]]. R. Kallosh, A. Linde and D. Roest, JHEP 1408, 052 (2014) [arXiv:1405.3646 [hep-th]].
[6] A. A. Starobinsky, Phys. Lett. B 91, 99 (1980). V. F. Mukhanov and G. V. Chibisov, JETP Lett. 33, 532 (1981). A. A. Starobinsky, Sov. Astron. Lett. 9, 302 (1983). B. Whitt, Phys. Lett. B 145, 176 (1984). L. A. Kofman, A. D. Linde and A. A. Starobinsky, Phys. Lett. B 157, 361 (1985).
[7] A. S. Goncharov and A. D. Linde, Sov. Phys. JETP 59, 930 (1984). A. B. Goncharov and A. D. Linde, Phys. Lett. B 139, 27 (1984). A. Linde, JCAP 1502, no. 02, 030 (2015) [arXiv:1412.7111 [hep-th]].
[8] D. S. Salopek, J. R. Bond and J. M. Bardeen, Phys. Rev. D40, 1753 (1989). F. L. Bezrukov and M. Shaposhnikov, Phys. Lett. B 659, 703 (2008) [arXiv:0710.3755 [hep-th]]. R. Fakir and W. G. Unruh, Phys. Rev. D 41, 1783 (1990). D. I. Kaiser, Phys. Rev. D 52, 4295 (1995) [astro-ph/9408044]. J. L. Cervantes-Cota and H. Dehnen, Nucl. Phys. B 442, 391 (1995) [astro-ph/9505069]. E. Komatsu and T. Futamase, Phys. Rev. D 59, 064029 (1999) [astro-ph/9901127]. S. Ferrara, R. Kallosh, A. Linde, A. Marrani and A. Van Proeyen, Phys. Rev. D 83, 025008 (2011) [arXiv:1008.2942 [hep-th]]. S. Ferrara, R. Kallosh, A. Linde, A. Marrani and A. Van Proeyen, Phys. Rev. D 82, 045003 (2010) [arXiv:1004.0712 [hep-th]]. A. Linde, M. Noorbala and A.Westphal, JCAP 1103, 013 (2011) [arXiv:1101.2652 [hep-th]]. R. Kallosh and A. Linde, JCAP 1306, 027 (2013) [arXiv:1306.3211 [hep-th]].
[9] E. Silverstein and A. Westphal, "Monodromy in the CMB: Gravity Waves and String Inflation", Phys. Rev. D78 (2008) 106003 [arXiv:0803.3085]; L. McAllister, E. Silverstein and A. Westphal, Gravity Waves and Linear Inflation from Axion Monodromy, Phys. Rev. D82 (2010) 046003 [arXiv:0808.0706]; J. P. Conlon, Brane-Antibrane Backreaction in Axion Monodromy Inflation, JCAP 1201 (2012) 033 [arXiv:1110.6454]; R. Flauger, L. McAllister, E. Pajer, A. Westphal and G. Xu, Oscillations in the CMB from Axion Monodromy Inflation, JCAP 1006 (2010) 009 [arXiv:0907.2916]; S. Hannestad, T. Haugbolle, P. R. Jarnhus and M. S. Sloth, Non-Gaussianity from Axion Monodromy Inflation, JCAP 1006 (2010) 001 [arXiv:0912.3527]; R. Flauger, L. McAllister, E. Silverstein, A. Westphal, Drifting Oscillations in Axion Monodromy, arXiv:1412.1814; T.C. Bachlechner, C. Long, and L. McAllister, Planckian Axions and the Weak Gravity Conjecture, JHEP bf 1601 (2016) 091 [arXiv:1503.07853]; J. Brown, W. Cottrell, G. Shiu, and P. Soler, Tunneling in Axion Monodromy, 1. arXiv:1607.00037.
[10] P. A. R. Ade et al. Astron. Astrophys. 571, A22 (2014) [arXiv:1303.5082 [astro-ph.CO]]. P. A. R. Ade et al., arXiv:1502.02114 [astro-ph.CO]. P. A. R. Ade *et al.* [Planck Collaboration], arXiv:1502.01589 [astro-ph.CO].

[11] S. Ferrara, R. Kallosh and A. Linde, JHEP 10 143 (2014) [arXiv:1408.4096]. I. Antoniadis, E. Dudas, S. Ferrara and A. Sagnotti, Phys. Lett. B 733 32 (2014) [arXiv:1403.3269]. R. Kallosh and A. Linde, JCAP 01 025 (2015) [arXiv:1408.5950]. G. Dall'Agata and F. Zwirner, JHEP 12 172 (2014) [arXiv:1411.2605]. R. Kallosh, A. Linde and M. Scalisi, JHEP 03 111 (2015) [arXiv:1411.5671]. A.B. Lahanas and K. Tamvakis, Phys. Rev. D 91 085001 (2015) [arXiv:1501.06547]. R. Kallosh and A. Linde, Planck, Phys. Rev. D 91 083528 (2015) [arXiv:1502.07733]. J.J.M. Carrasco, R. Kallosh and A. Linde, JHEP 10 147 (2015) 147 [arXiv:1506.01708].

[12] E. V. Linder, Phys. Rev. D 91, 123012 (2015) [arXiv:1505.00815].

[13] R. R. Caldwell and E. V. Linder, Phys. Rev. Lett. 95, 141301 (2005) [astro-ph/0505494].

[14] M. Shahalam, S. Sami, A. Agarwal, Mon. Not. R. Astron. Soc. 448, 2948−2959 (2015) [arXiv:1501.04047].

[15] R. Myrzakulov and M. Shahalam, Gen. Rel. Grav. 47, 81 (2015).

[16] N. Suzuki, D. Rubin, C. Lidman, G. Aldering, R. Amanullah, K. Barbary, L. F. Barrientos and J. Botyanszki *et al.*, Astrophys. J. **746**, 85 (2012) [arXiv:1105.3470 [astro-ph.CO]].

[17] R. Lazkoz, S. Nesseris, L. Perivolaropoulos, J. Cosmol. Astropart. Phys., 0511, 010 (2005)

[18] O. Farooq and B. Ratra, Astrophys. J. **766**, L7 (2013) [arXiv:1301.5243 [astro-ph.CO]].

[19] P. A. R. Ade *et al.* [Planck Collaboration], arXiv:1303.5076 [astro-ph.CO].

[20] C. Zhang, H. Zhang, S. Yuan, T. -J. Zhang and Y. -C. Sun, arXiv:1207.4541 [astro-ph.CO].

[21] J. Simon, L. Verde and R. Jimenez, Phys. Rev. D **71**, 123001 (2005) [astro-ph/0412269].

[22] M. Moresco, L. Verde, L. Pozzetti, R. Jimenez and A. Cimatti, JCAP **1207**, 053 (2012) [arXiv:1201.6658 [astro-ph.CO]].

[23] C. -H. Chuang and Y. Wang, arXiv:1209.0210 [astro-ph.CO].

[24] C. Blake, S. Brough, M. Colless, C. Contreras, W. Couch, S. Croom, D. Croton and T. Davis *et al.*, Mon. Not. Roy. Astron. Soc. **425**, 405 (2012) [arXiv:1204.3674 [astro-ph.CO]].

[25] D. Stern, R. Jimenez, L. Verde, M. Kamionkowski and S. A. Stanford, JCAP **1002**, 008 (2010) [arXiv:0907.3149 [astro-ph.CO]].

[26] N. G. Busca, T. Delubac, J. Rich, S. Bailey, A. Font-Ribera, D. Kirkby, J. M. Le Goff and M. M. Pieri *et al.*, Astron. Astrophys. **552**, A96 (2013) [arXiv:1211.2616 [astro-ph.CO]].

[27] C. Blake, E. Kazin, F. Beutler, T. Davis, D. Parkinson, S. Brough, M. Colless and C. Contreras *et al.*, Mon. Not. Roy. Astron. Soc. **418**, 1707 (2011) [arXiv:1108.2635 [astro-ph.CO]].

[28] W. J. Percival *et al.* [SDSS Collaboration], Mon. Not. Roy. Astron. Soc. **401**, 2148 (2010) [arXiv:0907.1660 [astro-ph.CO]].

[29] F. Beutler, C. Blake, M. Colless, D. H. Jones, L. Staveley-Smith, L. Campbell, Q. Parker and W. Saunders *et al.*, Mon. Not. Roy. Astron. Soc. **416**, 3017 (2011) [arXiv:1106.3366 [astro-ph.CO]].

[30] N. Jarosik, C. L. Bennett, J. Dunkley, B. Gold, M. R. Greason, M. Halpern, R. S. Hill and G. Hinshaw *et al.*, Astrophys. J. Suppl. **192**, 14 (2011) [arXiv:1001.4744 [astro-ph.CO]].

[31] D. J. Eisenstein *et al.* [SDSS Collaboration], Astrophys. J. **633**, 560 (2005) [astro-ph/0501171].

[32] R. Giostri, M. V. d. Santos, I. Waga, R. R. R. Reis, M. O. Calvao and B. L. Lago, JCAP **1203**, 027 (2012) [arXiv:1203.3213 [astro-ph.CO]].

[33] E. Komatsu et al., ApJS 192, 18 (2011).

[34] W. Hu and N. Sugiyama, Astrophys. J 471, 30 (1996).